# $\phi$ production in $\pi^- p$ collisions near threshold*

H. Courant, Y. I. Makdisi, M. L. Marshak, E. A. Peterson, K. Ruddick, and J. Smith-Kintner†
*School of Physics and Astronomy, University of Minnesota, Minneapolis, Minnesota 55455*
(Received 5 January 1977)

Using a secondary pion beam from the Argonne Zero Gradient Synchrotron we have studied the process $\pi^- p \to \phi n$ in the region of the cross-section enhancement near kinematic threshold. For incident momenta between 1.6 and 2 GeV/$c$, we have determined production and decay angular distributions and extrapolated total cross sections from a sample of about 160 $\phi$'s above background. The production and decay distributions are consistent with isotropy over this entire incident-momentum range. The extrapolated total cross section varies between 19 and 25 $\mu$b.

The production of $\phi$ mesons in $\pi^- p$ collisions provides an interesting demonstration of both the power and the limitations of simple quark models. If the $\phi$ meson were a pure $\lambda\bar{\lambda}$ quark state, its production in $\pi^- p$ collisions would be forbidden by the Okubo-Zweig-Iizuka (OZI) rule[1] owing to the absence of strange quarks in the initial state. To the extent that the $\omega$-$\phi$ mixing angle is such that the $\phi$ has some small admixture of $\mathcal{P}$ and $\mathcal{N}$ quarks, the reaction $\pi^- p \to \phi n$ should occur, but the cross section should be (and is) suppressed relative to the cross section for the reaction $\pi^- p \to \omega n$. One limitation of this simple quark model is that it does not explain the different energy dependences of the $\omega$ and the $\phi$ cross sections. $\omega$ production drops uniformly from near threshold, proportional to $s^{-2.5}$. The $s$ dependence of the total $\phi$ production cross section is less clear because the relatively flat $t$ dependence results in large angular extrapolations from the measured data.[2] However, $d\sigma/dt$ at $t=0$ is well known; this cross-section has a threshold enhancement, drops sharply in the $p_0 = 3$ to 5 GeV/$c$ region, and then has an $s^{-2}$ dependence at higher incident momenta.

We have performed an experiment in Beam 8 of the Argonne Zero Gradient Synchrotron (ZGS) in order to study this threshold enhancement by making measurements of the total cross section and determining the production and decay angular distributions of the $\phi$ mesons. The $\phi$'s were detected by measuring the momentum and angles of candidate $K^+K^-$ pairs produced in the target and reconstructing the effective mass. The recoil neutron was not detected; but for acceptable events, the calculated missing mass was required to approximate the nucleon mass. By then assuming the mass of the neutron, this technique yielded a one-constraint (1-C) fit. In order to minimize losses due to the decay of the low-momentum $K$ mesons produced in this experiment, the apparatus was arranged compactly. Both the target and all of the detectors were located in the magnetic field of a wide-aperture analyzing magnet.

The layout of the experiment is shown in Fig. 1. A secondary beam of 1 to $3\times10^5$ particles per

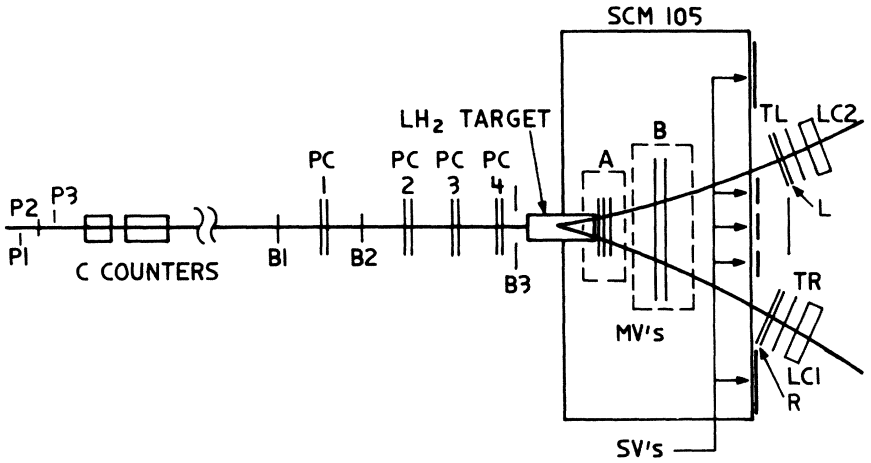


FIG. 1. The layout of the experimental apparatus.

burst was incident on a 30-cm liquid hydrogen target. The momenta of the incoming particles were measured to an accuracy of ± 0.5 percent by a three-counter, overlapping hodoscope ($P1$, $P2$, $P3$) located at the intermediate focus of the beam; the particles were identified as pions by two Freon-filled, threshold Čerenkov counters. The angles and positions of the incident particles were determined by four $x$-$y$ multiwire proportional chamber (MWPC) planes ($PC1$, $PC2$, $PC3$, $PC4$). The analyzing magnet (SCM-105) produced a maximum field integral of 11.4 kG m with an aperture 0.7-m high by 2-m wide. The trajectories of the final-state particles were measured at three points each by $x$ and $y$ MWPC planes ($A, B, R, L$) and at one point by a $u$ plane (inclined at 30° to the vertical) to resolve reconstruction ambiguities. The chamber spatial resolutions were ± 1.5 mm.

The trigger consisted of a coincidence of beam scintillation counters ($B1$ and $B2$), scintillation counters $TL$ and $TR$, located just downstream of the final MWPC planes, and the absence of signals from beam halo counter $\overline{B3}$, downstream veto counters $\overline{SV}$ and the $\overline{MV}$ veto counters, which obscured the pole faces and sides of the analyzing magnet downstream of the target. All of the veto counters, except for $\overline{B3}$ and the $\overline{SV}$ counter directly in the path of the uninteracted beam, contained lead-scintillator sandwiches to reject photons as well as charged particles. To discriminate against the substantial background from $\pi^+\pi^-$ events, the trigger included in anticoincidence two Lucite Čerenkov counters ($LC1$ and $LC2$) of somewhat novel design, one located behind each of the final MWPC planes. These counters were basically of the Fitch type,[3] but the 5-cm-thick radiator was painted black at one end and could be tilted to adjust the threshold over the range $0.85 < \beta < 0.95$. The tilting of the counter changed the detection threshold by altering the relationship between the Čerenkov angle and the angle for total internal reflection. (See Fig. 2). The change in detection efficiency with $\beta$ as determined by calibration runs with these counters placed in the incident beam is shown in Fig. 3. The combined rejection efficiency of both Lucite Čerenkov counters against pion pairs was 25:1. The overall trigger rate for the system $B1 \cdot B2 \cdot \overline{B3} \cdot TR \cdot TL \cdot \overline{MV} \cdot \overline{SV}$ varied between 3.6 and 8 triggers per $10^5$ incident particles, with the highest trigger rate at the highest incident momentum.

The data were recorded with different angular settings of the spectrometer arms and different tilt angles for the $LC$ counters for each of the four incident momenta. A fraction of the events were analyzed on-line by a PDP-9 computer and all data were written on magnetic tape for later analysis. This off-line analysis consisted of reconstructing the momenta and angles of the incident and scattered particles using the position measurements from the MWPC's and the measured

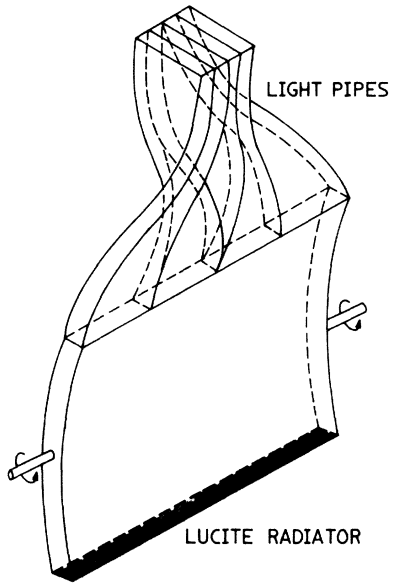


FIG. 2. A schematic diagram of the radiator in the Lucite Čerenkov counters. Because the bottom is painted black only the light emitted upward can reach the photomultiplier tube. Light which is not totally internally reflected in the Lucite is absorbed by a black shroud (not shown) and is not detected.

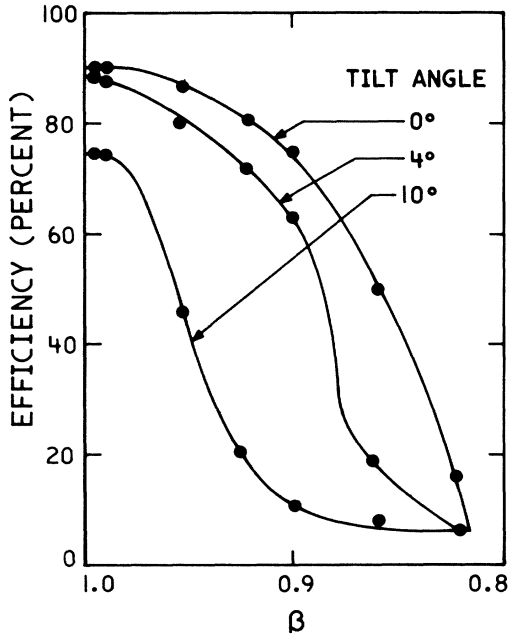


FIG. 3. The detection efficiency for the Lucite Čerenkov counter as a function of $\beta$ for the particle and the tilt angle of the counter.

field map for the analyzing magnet. Events with more than two charged particles in the final state were rejected. Those remaining were interpreted according to the kinematic hypothesis $\pi^- p \to K^+ K^- X$. Those events for which the mass of $X$ was less than 75 MeV from the neutron mass were used for a 1-C fit to the hypothesis $\pi^- p \to K^+ K^- n$, where the mass of the neutron was assumed in the fitting. Events with a $\chi^2$ confidence less than 10 percent were rejected after this step. The remaining events in each bin of incident momentum and four-momentum transfer were separately histogrammed as a function of effective mass; after correction for the acceptance of the apparatus, which was determined by Monte Carlo calculation assuming isotropic decays, the effective mass distributions were fitted to a Breit-Wigner resonance and a phase-space background. Because of the experimental resolution of ~10 MeV full width at half maximum (FWHM), the width of the resonance was left as a floating parameter in the fit. The total data sample of $3.1 \times 10^5$ triggers yielded about 160 $\phi$'s above background after this procedure (Table I). A typical effective mass distribution is shown in Fig. 4; although the histogram has been corrected for the spectrometer acceptance, it has been normalized such that the number of events shown in the $\phi$ region corresponds to the number of events actually observed. The solid lines show the results of the fit for the resonance and the phase-space background. The fit parameters were used to calculate cross sections for each value of $s$ and $t$.

The uncertainties in the results of the experiment come from both systematic and statistical origins. The former were estimated from the size and method of computation of the corrections applied to the data, which are listed in Table I. The largest of these factors are kaon decay, which was determined by Monte Carlo calculation, the $\phi \to K^+ K^-$ branching ratio, which comes from published data, and proportional-chamber inefficiency. The large inefficiency correction was a result of

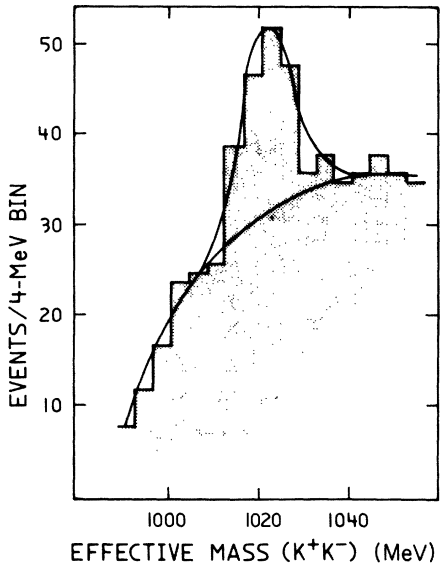


FIG. 4. The $K^+ K^-$ effective mass distribution for events with an incident momentum of 1.8 GeV/$c$ and a neutron missing mass. The distribution has been corrected by the spectrometer acceptance determined from Monte Carlo calculation and has been normalized so that the number of events in the $\phi$ region corresponds to the number of events actually observed. The lines represent fits to the resonance and the background.

the stringent requirements placed on each track candidate in order to permit a measurement of the momentum. Since there were only three MWPC $x$-$y$ planes and one $u$ plane, small individual plane inefficiencies considerably lowered the overall efficiency of the spectrometer. Because this was a large effect, it was determined by measuring the single plane inefficiency for each plane in known good events and combining these individual detection probabilities into a net spectrometer probability in the usual way. These effects were constant over the acceptance, but they did vary with time, so the corrections were applied to the data on a run-by-run basis. The other correction

TABLE I. Correction factors applied to the data.

| Source | Factor | Origin |
|---|---|---|
| Proportional-chamber inefficiency | 2.50–2.86 | Measured |
| Kaon decay | 1.89–2.44 | Calculated |
| Branching ratio ($\phi \to K^+ K^-$) | 2.13 | Published data |
| Vetoing of $K$'s in $LC$ counters | 1.18 | Measured |
| Analysis cuts | 1.10 | Calculated |
| Vetoing of $\delta$ rays | 1.09 | Calculated |
| Beam lepton contamination | 1.04–1.07 | Measured |
| Vetoing of neutrons | 1.02 | Calculated |
| Deadtime | 1.02 | Measured |
| Nuclear absorption | 1.01–1.02 | Calculated |

TABLE II. Differential cross sections and extrapolated total cross sections for the reaction $\pi^- p \to \phi n$ as determined in this experiment.

| Beam momentum | $10^{-6}\times$ (No. of $\pi$'s) | $10^3\times$ (Fractional acceptance[a]) | No. of $\phi$'s | $d\sigma/d\Omega^*$ ($\theta^*=0$) ($\mu$b/sr) | $\sigma(\pi p \to \phi n)$ ($\mu$b) |
|---|---|---|---|---|---|
| 1.6 | 1310 | 4.6 | 23 | 1.5±0.5 | 19±6 |
| 1.7 | 1877 | 4.1 | 38 | 1.9±0.5 | 24±7 |
| 1.8 | 3201 | 4.9 | 80 | 2.0±0.5 | 25±8 |
| 2.0 | 997 | 6.2 | 28 | 1.7±0.5 | 21±7 |

[a] This acceptance includes geometrical factors and $K$-decay probabilities but none of the other factors included in Table I.

factors were relatively small and were determined as indicated in Table I. The effects of accidental tracks and random vetoing were measured and found to be negligible as a result of the low beam intensity. The overall systematic error, determined by adding the errors in the individual corrections in quadrature, was 16 percent. The differential cross sections listed in Table II include this systematic error and the statistical errors due to the limited number of $\phi$ events and the background subtraction added in quadrature.

The angular distribution for $\phi$ production in the center-of-mass system is shown in Fig. 5, with events at incident pion momenta from 1.6 to 2.0 GeV/$c$ combined. Over the angular range accessible to this experiment, the data appear to have a slight dependence on $\cos\theta^*$, but they are, in fact, not inconsistent with the isotropic production

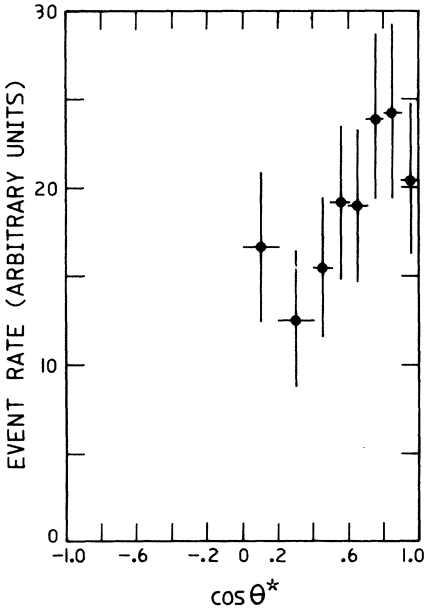


FIG. 5. The center-of-mass production angle for events satisfying the hypothesis $\pi^- p \to \phi n$ for incident momenta between 1.6 and 2.0 GeV/$c$. Backgrounds have been subtracted in each angular range.

reported in other experiments at low incident momenta.[2,4] For $0.4 < \cos\theta^* < 1.0$, where the acceptance is large, the $\chi^2$ for pure $S$-wave production is 2.9 for 5 degrees of freedom. The decay angular distributions for $\phi \to K^+K^-$, corrected for acceptance, are shown in Fig. 6, with all events at incident momenta between 1.7 and 2.0 GeV/$c$ included. The events at $p_0 = 1.6$ GeV/$c$ have been excluded from these plots because of the difficulty in fitting the background adjacent to the kinematic threshold. The angles for each event are computed in the Gottfried-Jackson frame using the usual definitions for $\theta$ and $\phi$, the Treiman-Yang angle. The $\theta$ distribution is summed over $\phi$; the $\phi$ distribution is summed over $\theta$. These distributions are also consistent with isotropy, even though events with different values of $t$ for $\phi$ production are included; the $\chi^2$ for $\sigma(\cos\theta) = \text{constant}$ is 9.8 for 7 degrees of freedom and the $\chi^2$ for $\sigma(\phi) = \text{constant}$ is 0.9 for five degrees of freedom. If we assume isotropy in both production and decay angular distributions, which is certainly consistent with the data, we can calculate from the observed events the total cross section for the process $\pi^- p \to \phi n$. These cross sections are listed in Table II; a nonisotropic production cross section would tend to lower these numbers. Figure 7 displays this cross-section data along with previous measurements.[2,4,5] Since in most $\phi$-production experiments, including the one reported here, only a portion of the angular distribution is observed, the plot indicates only that part of the cross section obtained by integrating out to $|t'| = 0.9$ (GeV/$c$)$^2$.

The model of Berger and Sorensen[6] explains the threshold enhancement in $\pi^- p \to \phi n$ in terms of $s$-channel threshold and duality cancellations in the intermediate states of $K^*(890)$ and $K^{**}(1420)$ in a box diagram, which obeys the OZI rule at each vertex. In their view, the threshold enhancement arises because the $K^{**}(1420)$ is energetically forbidden as an intermediate state near kinematic threshold; above 2 GeV/$c$, where the $K^{**}(1420)$ contribution is permitted, it cancels the ampli-

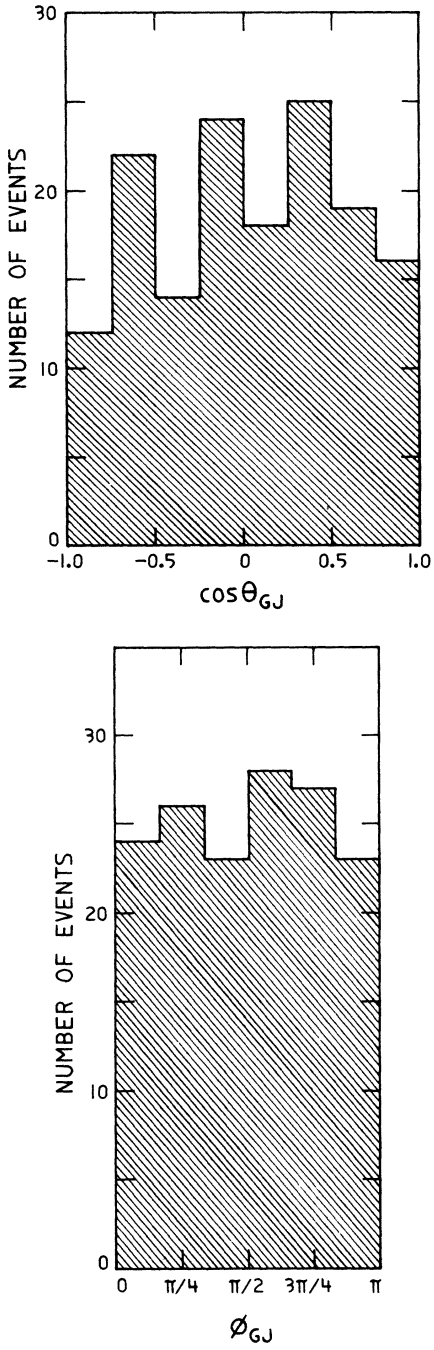


FIG. 6. The decay angles in the Gottfried-Jackson frame for the $\phi$ mesons. Events with an incident momentum between 1.7 and 2 GeV/$c$ are summed together. The plots are corrected for acceptance. The $\theta$ distributions are averaged over $\phi$ and the $\phi$ distributions are averaged over $\theta$.

tude resultant from the $K^*(890)$ intermediate state leading to a small, net scattering amplitude. Their model predicts relatively flat angular distributions, which is in agreement with these data.

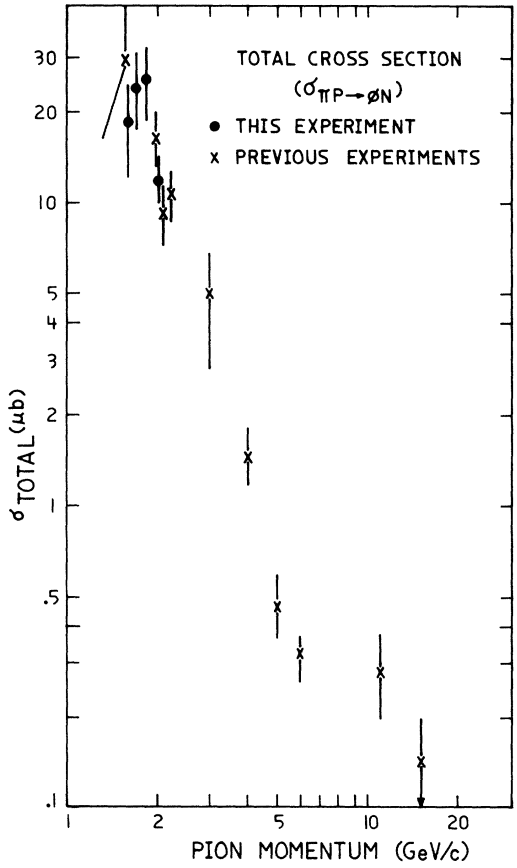


FIG. 7. The cross section for the process $\pi^- p \to \phi n$ as a function of the incident pion momentum. The differential cross section has been integrated only to $|t'| = 0.9$ (GeV/$c$)$^2$ to obtain the plotted cross sections.

However, their use of only one graph in the explicit calculation accounts for only about 10 percent of the experimental cross section and results in a forward dip which is not observed. The inadequacy of the use of only one graph in their model is also demonstrated by the decay angular distributions. This one graph implies that the $\phi$ would be produced with helicity one[7] and would therefore have a decay distribution that varied as $\cos^2\theta$. The observed decay distribution is not consistent with this prediction and indicates that calculations in the context of the Berger-Sorensen model must consider other intermediate states. In the future, it may be interesting to compare these results with measurements near threshold for the process $\pi^- p \to \psi n$, for which only an upper limit now exists.[8] This latter reaction also violates the OZI rule in that charmed quarks are also not present in the initial state.

We thank the entire staff of the Argonne ZGS for assistance in running this experiment.

*Work supported by the U. S. Energy Research and Development Administration.

†Present address: Wilson Synchrotron Laboratory, Cornell University, Ithaca, New York 14850.

[1]S. Okubo, Phys. Lett. 5, 165 (1963); G. Zweig, CERN Report No. CERN-TH 402, 1964 (unpublished); J. Iizuka, Prog. Theor. Phys. Suppl. 37-38, 21 (1966); J. Rosner, Phys. Rev. Lett. 32, 1463 (1974).

[2]D. S. Ayres *et al.*, Phys. Rev. Lett. 32, 1463 (1974); D. Cohen *et al.*, *ibid.* 38, 269 (1977).

[3]V. Fitch and R. Motley, Phys. Rev. 101, 496 (1956).

[4]O. I. Dahl *et al.*, Phys. Rev. 163, 1377 (1967); M. A. Abolins, in *Proceedings of the International Conference on Elementary Particles, Heidelberg, 1967*, edited by H. Filthuth (North-Holland, Amsterdam, 1968), p. 509; D. Bollini *et al.*, Nuovo Cimento 60A, 541 (1969); J. H. Boyd *et al.*, Phys. Rev. 166, 1458 (1968); B. D. Hyams *et al.*, Nucl. Phys. B22, 189 (1970).

[5]H. H. Williams, SLAC Report No. 142, 1972 (unpublished).

[6]E. L. Berger and C. Sorensen, Phys. Lett. 62B, 303 (1976).

[7]C. Sorensen, private communication.

[8]R. Klem *et al.*, unpublished work.

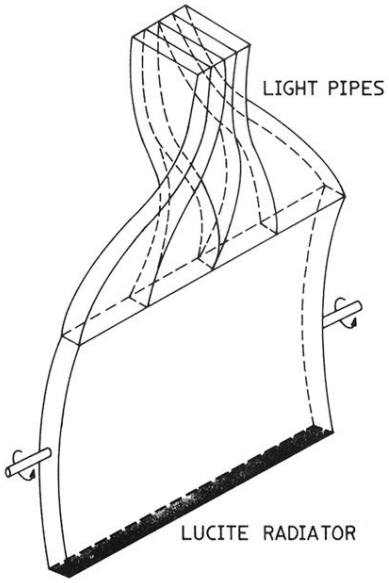


FIG. 2. A schematic diagram of the radiator in the Lucite Cerenkov counters. Because the bottom is painted black only the light emitted upward can reach the photomultiplier tube. Light which is not totally internally reflected in the Lucite is absorbed by a black shroud (not shown) and is not detected.

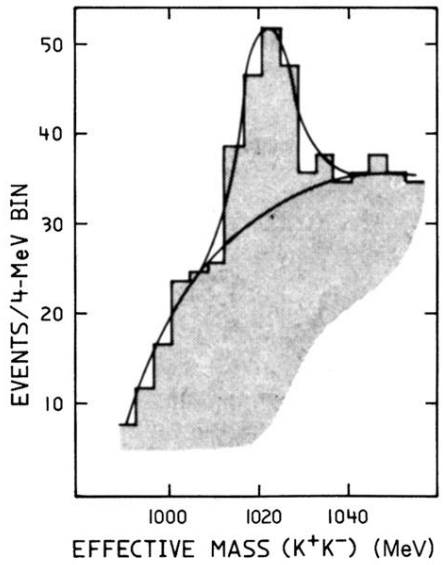


FIG. 4. The $K^+K^-$ effective mass distribution for events with an incident momentum of 1.8 GeV/$c$ and a neutron missing mass. The distribution has been corrected by the spectrometer acceptance determined from Monte Carlo calculation and has been normalized so that the number of events in the $\phi$ region corresponds to the number of events actually observed. The lines represent fits to the resonance and the background.